3D Numerical Modeling of Geyser Formation by Release of Entrapped Air from Horizontal Pipe into Vertical Shaft

S. N. Chan[1]; J. Cong[2]; and Joseph H. W. Lee, F.ASCE[3]

Abstract: Geysers are explosive eruptions of air-water mixture from manholes in drainage systems. When the design capacity of urban storm water drainage systems is exceeded during extreme rainfall, rapid inflows into the drainage network can lead to air-water interactions that give rise to geysers—causing damage to the water infrastructure and threatening human lives. Although extensive research has revealed the role of entrapped air in causing large pressure transients in drainage tunnels, the mechanism of geyser formation remains elusive. In this study, an unsteady three-dimensional (3D) computational fluid dynamics (CFD) model is developed to simulate the pressure transients and air-water interactions during geyser events using the volume-of-fluid (VOF) technique. Extensive numerical simulations are conducted to study the air-pocket dynamics caused by release of trapped air from a horizontal tunnel into a vertical riser. Model predictions of the air-water interface in the vertical shaft are in good agreement with laboratory measurements by a high-speed camera; the mechanism for the formation of geysers is elucidated. It is found that during a geyser event, compression of the air pocket in the riser can lead to rapid acceleration of the overlying water column and its expulsion from the riser; the air-pocket pressure is significantly higher than the hydrostatic pressure of the overlying water column, and the velocity is greater than that of a Taylor bubble. Comprehensive numerical modeling has been conducted to study the effect of the vertical shaft diameter, the upstream pressure head and the air-pocket volume on the air-pocket dynamics; the results show that geyser formation is primarily controlled by the riser to tunnel diameter ratio, D_r/D. 3D CFD simulations have also been carried out for an idealized prototype drainage system; it is shown that the geyser behavior can be characterized by extremely large vertical air velocities that result in dispersed air-water mixtures often observed in the field. **DOI: 10.1061/(ASCE)HY.1943-7900.0001416.**

Author keywords: Geyser; Urban drainage; Hydraulic transients; Air-water interaction; Volume-of-fluid (VOF); Computational fluid dynamics (CFD) model.

Introduction

Geysers are explosive eruptions of air-water mixture from manholes in drainage systems. When the design capacity of urban storm water drainage systems is exceeded during heavy rainfall, rapid inflows into the drainage network can lead to air-water interactions that give rise to geysers—causing damage to the water infrastructure and threatening human lives. Over the past two decades, geysers have been attributed to air-water interactions—in particular the presence of air pockets that can give rise to significant pressure surges (e.g., Hamam and McCorquodale 1982; Li and McCorquodale 1999; Martin 1976; Zhou et al. 2002a, b). More recently, systematic investigations have demonstrated the possibility of different types of air-water interactions as a function of riser and pipe diameters, and the rate of increase of inflows into an existing pipeline partially filled with water (Wright et al. 2011; Wright 2013, 2014; Vasconcelos and Wright 2012, 2008, 2011, 2016).

Whereas the previous studies have confirmed the role of entrapped air in causing large pressure transients, the mechanism of geyser formation remains elusive, primarily because of the lack of detailed observations. In particular, the physical mechanisms under which geysers are formed have not been conclusively reported or elucidated. A comprehensive series of laboratory experiments has recently been performed on a physical model of a simplified drainage system (Cong 2016; Cong et al. 2017), which consists of a vertical riser and a horizontal pipe connected to a constant head tank. The system is filled with water; an air pocket is then released into the horizontal pipe. The trajectories of the air pockets in the horizontal pipe and vertical riser are measured by a high speed camera, and pressures are measured at key locations. The experiments show that the vertical air-pocket motion in a geyser differs greatly from that of a Taylor bubble—an air pocket rising steadily in a vertical tube under buoyancy with a thin water film around it (Davies and Taylor 1950); the mechanism of geyser formation in the laboratory set up is elucidated. The importance of the ratio of riser to pipeline diameter, and the volume of air in geyser formation was also demonstrated (Cong et al. 2017).

Whereas important insights can be gained from the small-scale experiments, the extrapolation of the laboratory results to the prototype is a difficult task that may be assisted by 3D numerical modeling. It is well-recognized that computational fluid dynamics (CFD) modeling is useful in capturing greater details of the physical processes than 1D models based on the rigid column hypothesis. Nevertheless, the resolution of the fine scale flow processes (e.g., Taylor bubble) imposes significant computational

[1]Research Assistant Professor, Dept. of Civil and Environmental Engineering, and Junior Fellow, Institute for Advanced Study, Hong Kong Univ. of Science and Technology, Clear Water Bay, Hong Kong, China.

[2]Formerly, M.Phil. Student, Dept. of Civil and Environmental Engineering, Hong Kong Univ. of Science and Technology, Clear Water Bay, Hong Kong, China.

[3]Chair Professor, Dept. of Civil and Environmental Engineering, Hong Kong Univ. of Science and Technology, Clear Water Bay, Hong Kong, China (corresponding author). E-mail: jhwlee@ust.hk

Note. This manuscript was submitted on May 15, 2017; approved on August 16, 2017; published online on December 22, 2017. Discussion period open until May 22, 2018; separate discussions must be submitted for individual papers. This paper is part of the ***Journal of Hydraulic Engineering***, © ASCE, ISSN 0733-9429.

constraints; the formulation of the 3D numerical model is also not straightforward—there has hitherto been relatively very few attempts at CFD modeling of the geyser flow. Zhou et al. (2011) performed two-dimensional (2D) volume of fluid (VOF) calculations on the transient flow of an air pocket trapped in a hypothetical pipeline; the computed pressure variation compared well with experimental measurements. Catano-Lopera et al. (2014) conducted 3D two-phase flow calculations to study the occurrence of geysers for a small section of the Chicago tunnel and reservoir plan (TARP) system. Although the surging of the air-water mixture in the vertical riser is demonstrated, the physics of the geyser flow in the riser cross section remains unresolved. For example, the details of the water film flow surrounding the rising air pocket—which is intimately connected with the rapid transient nature of geysers—is not resolved. Overall, there has been very few detailed numerical studies of geysers, and the mechanism of geyser flow has not been successfully modeled.

This paper presents a CFD study on geyser events using the two-phase VOF technique. Guided by recent experiments by Cong et al. (2017), the set-up of the CFD model will first be described. The computed detailed air-water interface motion in the vertical riser is presented and compared with experimental data. The mechanism for the formation of a geyser is elucidated for the first time along with the conditions that will likely lead to geyser events. A numerical study is also conducted to examine the effect of shaft diameter, upstream pressure head, and the air volume impact on the formation of geysers. Finally, the model is used to compute an idealized section of a drainage system using prototype dimensions; the differences between the prototype and laboratory geysers are discussed.

3D Numerical (CFD) Model

Governing Equations

The VOF model can simulate two immiscible fluids (water and air) by solving a single set of momentum equations and tracking the volume fraction of each of the fluids throughout the domain (Hirt and Nichols 1981). The tracking of the interface between the phases is accomplished by the solution of a continuity equation for the volume fraction of one of the phases. For the water phase, this equation has the following form:

$$\frac{\partial}{\partial t}(\alpha_w \rho_w) + \nabla \cdot (\alpha_w \rho_w \mathbf{U}) = 0 \tag{1}$$

where α_w = volume fraction for the water phase. The volume fraction for the air phase α_a will be computed based on the constraint of:

$$\alpha_a + \alpha_w = 1$$

In a two-phase system, the average density in each cell is given by

$$\rho = \alpha_w \rho_w + (1 - \alpha_w)\rho_a \tag{2}$$

A single momentum equation is solved throughout the domain, and the resulting velocity field $\mathbf{U} = (u,v,w)$ is shared among the phases. The momentum equation below, is dependent on the volume fractions of all phases through the properties ρ and μ_t.

$$\frac{\partial}{\partial t}(\rho \mathbf{U}) + \nabla \cdot (\rho \mathbf{U}\mathbf{U}) = -\nabla P + \nabla \cdot [\mu_t(\nabla \mathbf{U} + \nabla \mathbf{U}^{\mathrm{T}})] + \rho \mathbf{g} \tag{3}$$

The turbulent dynamic viscosity μ_t is determined using the standard $k - \epsilon$ turbulence model. $\mathbf{g} = (0,0,-9.81)$ = gravitational acceleration.

The density of air ρ_a is related to the air pressure using the ideal gas law. For compressible flows, the ideal gas law is written as:

$$\rho_a = \frac{P_{op} + P}{\frac{R}{M_w}T} \tag{4}$$

where P_{op} = operating pressure defined as the atmospheric pressure $P_{\mathrm{atm}} = 101.325\,\mathrm{kPa}$, P = local relative (or gauge) pressure, $R = 8.314\ \mathrm{J/mol/K}$ = universal gas constant, and $M_w = 28.966\ \mathrm{g/mol}$ = molecular weight of air. The water phase is treated as incompressible with density $\rho_w = 998.2\ \mathrm{kg/m^3}$. The temperature T (in K) is computed from the conservation of energy (temperature) equation:

$$\frac{\partial}{\partial t}(\rho T) + \nabla \cdot (\rho T \mathbf{U}) = \nabla \cdot \left[\frac{\mu_t}{\mathrm{Pr}}(\nabla T)\right] \tag{5}$$

where Pr = Prandtl number = 0.85.

The governing Eqs. (1) and (3) are solved numerically using the finite volume method in the commercial CFD code of *ANSYS FLUENT*. The PISO (pressure-implicit with splitting of operators) algorithm is employed for velocity-pressure correction with under-relaxation factor of 0.5 for pressure and momentum, 0.8 for k and ε, and 1.0 for density, temperature, and turbulent viscosity. A second order upwind advection scheme is used for momentum, density, and temperature, whereas a first order upwind advection scheme is used for k and ϵ. The volume fraction equation [Eq. (1)] is solved through the Geo-reconstruct scheme in *FLUENT* (Youngs 1982). In the geometric reconstruction approach, the standard second-order scheme is used to obtain the face fluxes whenever a cell is completely filled with one of the two phases. When the cell is near the interface between two phases, the geometric reconstruction scheme is used to determine the interface between fluids using a piecewise-linear approach from the volume fraction of adjacent cells. Except for the volume fraction equation, a first order implicit time stepping scheme is used for the marching of the solution with time. Convergence is declared when the normalized residual is less than 10^{-6} for temperature and 10^{-4} for all other variables. Typically, approximately 10–20 iterations are required for convergence in each time step.

Numerical Experiments

The laboratory experiments of Cong et al. (2017) are simulated under exactly the same conditions (Table 1). The physical model is a simplified drainage system, which consists of a vertical riser of diameter D_r and a horizontal pipe of diameter D connected to a constant head tank. The pipe is 6.6 m long with an inner diameter of $D = 0.05$ m. A riser of height 1.8 m and variable diameter ($D_r = 0.016 - 0.046$ m) is connected to the pipe with a T-junction at $x = 3.47$ m from the upstream. In the physical experiment, a number of valves are used to separate the pipe into different sections to allow experiments with different air volume. By opening or closing a selected valve, air pockets of different initial lengths (or volumes) can be formed.

Two series of numerical experiments were performed (Table 1), similar to those described in Cong et al. (2017). Two numerical experiments (Run A1 and Run A2) are dedicated to the condition without an external pressure [Series A, similar to those in Vasconcelos and Wright (2011)], the riser and horizontal pipe is filled with water to an initial head of H_0; the downstream section of the pipe is an air pocket of length L_0 and volume V_{air}.

Table 1. Summary of Key Parameters for Numerical Experiments

Run number	Tunnel diameter D (m)	Riser diameter D_r (m)	D_r/D	Initial (A)/upstream (B) pressure head H_0 (m)	Initial length of air pocket L_0 (m)	V_a/V_w[a]	Maximum height of rise[b] (m)	v_{net}[c] (m/s)	Geyser
				Series A, without upstream head					
A1[d]	0.05	0.016	0.32	0.88	0.61	6.77	0.80	0.270	No
A2[d]	0.05	0.040	0.80	0.88	1.80	4.26	0.85	0.320	No
				Series B, with upstream head					
B1[d]	0.05	0.016	0.32	0.88	0.61	6.77	2.48	0.420	Yes
B2	0.05	0.021	0.42	0.66	0.61	5.24	1.49	0.479	Yes
B3	0.05	0.026	0.52	0.66	0.61	3.42	1.41	0.521	Yes
B4	0.05	0.031	0.62	0.50	0.61	3.17	0.96	0.405	No
B5	0.05	0.031	0.62	0.66	0.61	2.40	1.28	0.492	Yes
B6	0.05	0.031	0.62	0.88	0.61	1.89	1.52	0.435	Yes
B7	0.05	0.031	0.62	1.00	0.61	1.59	1.64	0.460	Yes
B8	0.05	0.031	0.62	0.66	1.80	7.09	1.34	0.395	No
B9	0.05	0.031	0.62	0.88	1.80	5.32	1.82	0.435	Yes
B10	0.05	0.031	0.62	1.00	1.80	4.68	2.17	0.337	No
B11	0.05	0.036	0.72	0.66	0.61	1.78	1.23	0.421	No
B12	0.05	0.040	0.80	0.66	0.61	1.44	1.09	0.433	No
B13	0.05	0.040	0.80	0.66	1.80	4.26	1.21	0.474	No
B14[d]	0.05	0.040	0.80	0.88	1.80	3.20	1.57	0.454	No
B15	0.05	0.040	0.80	0.88	2.20	3.91	1.68	0.468	No
B16[e]	0.095	0.044	0.46	0.457	0.84	8.57	1.31	0.399	Yes

[a]$V_a = (\pi D^2/4)L_0$, volume of air in tunnel; $V_w = (\pi D_r^2/4)H_0$, volume of water in riser.
[b]Defined as the level where the air pocket breaks the free surface.
[c]v_{net} = net rising velocity of air pocket in the riser, relative to the free surface.
[d]Fine mesh is used.
[e]Experimental set up of Lewis (2011).

The upstream end of the pipe is a closed end. In the simulation, two riser diameters are tested: $D_r = 16$ mm (Run A1) and 40 mm (Run A2), with an initial pressure head of $H_0 = 0.88$ m, and $L_0 = 0.61$ and 1.8 m respectively. In the laboratory geysers are not observed for Series A experiments.

On the other hand, extensive numerical experiments are conducted with a pressurized pipe connected to a constant head reservoir (Series B) with the initial water depth in the riser at the same level. A total of 15 numerical experiments (Run B1–B15) are performed for different riser diameters, upstream head, and initial air volumes (Table 1) corresponding to the physical experiments (Cong et al. 2017). As an independent check, an additional numerical experiment (Run B16) is conducted for the experimental set up of Lewis (2011).

Model Grid

In the numerical model, the tunnel-riser system is discretized using approximately 100,000 boundary-fitting grid cells. A schematic diagram of the model is shown in Fig. 1. The tunnel cross section is discretized using 25 cells along the diameter, with finer grid size as the tunnel wall is approached. The riser diameter is discretized using approximately 50 cells, with smallest grid size of 0.1 mm; it is found that realistic simulation of the geyser dynamics requires a good resolution of the water film flow around the rising air pocket. The T-junction of the tunnel-riser system is discretized using tetrahedral cells, whereas the other parts of the tunnel and riser are discretized using hexahedral cells. To study the surging of the air-water mixture in the riser, a larger height of the riser (compared with the experiment) is adopted in the computational model (3.0 m) to confine the air pocket and water column within the riser during a geyser event. A relative coarse mesh (approximately 40,000 grid cells in total) is also used for a parametric numerical study on the effect of shaft diameter, air volume and upstream pressure on the formation of geyser.

Boundary and Initial Conditions

For Series A experiment without an upstream pressure head, both ends of the tunnel ($x = 0$ and 6.6 m, Fig. 1) are set as closed end walls. For Series B experiments, the upstream end of the tunnel is prescribed as a pressure inlet with pressure $= \rho_w g H_0$ and volume fraction of water = 1, to resemble the effect of the upstream reservoir. The top of the riser is prescribed as a pressure outlet of zero (atmospheric) pressure and volume fraction of water = 0. A smooth wall is assumed for the pipe wall with roughness length of 10^{-3} mm.

In the simulation, an air pocket of length L_0 (volume $= \pi L_0 D^2/4$) near the closed end of the tunnel and a water level of H_0 at the riser are prescribed. The initial temperature is assumed to be 300 K (26.85°C). The simulation starts at time $t = 0$, equivalent to the opening of the ball valve in the experiment. It is noted that in the simulation the opening of the valve is instantaneous, whereas in the experiment the valve opening time is approximately 0.5 s. The difference in valve opening time could result in a slightly early time of arrival of the air pocket at the riser, but the simulated pressure transient and air-water dynamics compare well with the experiment. Because the advection scheme of the VOF method is explicit, the Courant criteria have to be satisfied, and the maximum $Cr = (u\Delta t/\Delta x) = 0.75$, an adaptive time step is used with minimum $\Delta t = 10^{-5}$ s. The run time of a quad-core parallel computation on a Dell workstation with an Intel i4790 3.6 GHz CPU is approximately 360–400 h for a full simulation using the fine mesh. There may be a number of geysers when the air pocket cannot be ejected completely in a single geyser, and the strength of a geyser usually decreases with time. In this study, only the first geyser will be simulated. The simulation is stopped when the air pocket has

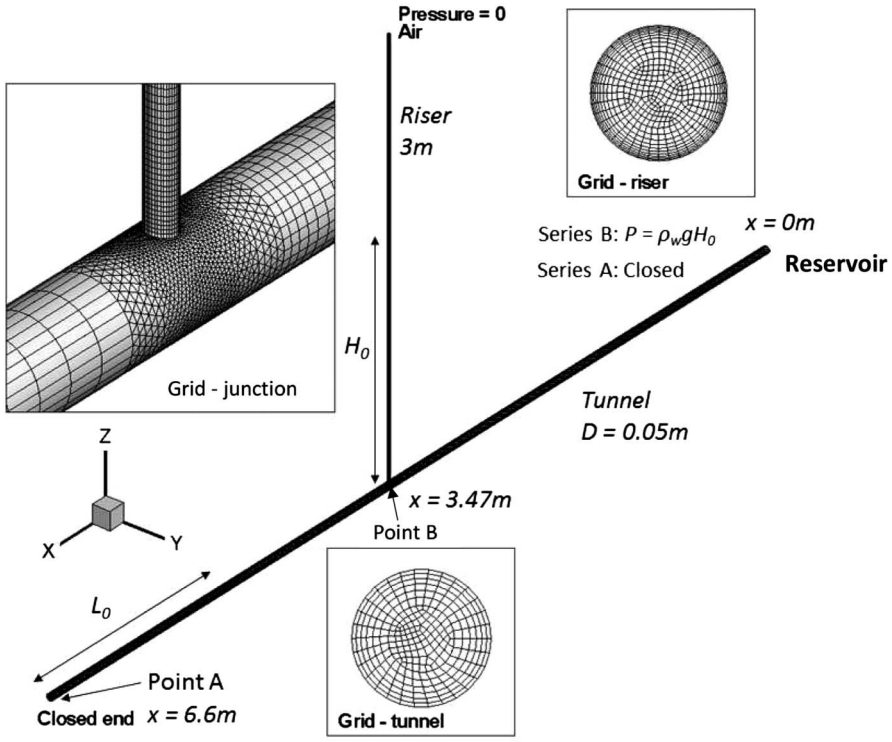

Fig. 1. Numerical model of laboratory experiment for study of air-water interaction in horizontal pipe with vertical riser

reached the free surface in the riser. When the coarse mesh is used, the run time is much reduced to approximately 50–70 h, yet the key features of air-pocket dynamics and geyser formation can still be faithfully captured.

Numerical Results

Air-Pocket Propagation in the Tunnel

In the numerical simulation, $t = 0$ corresponds to the time of valve opening. Fig. 2 shows the computed movement of an air pocket in the horizontal pipe after valve opening for a typical experiment of $D_r = 16$ mm (Series B, with upstream pressure; Run B1). Initially, the air pocket moves upstream like an air cavity in the upper half of the pipe, whereas the water propagates downstream as a dam-break wave [Figs. 2(a and b)]. When the water reaches the downstream end, the wave is reflected to form an upstream-moving hydraulic surge [Fig. 2(c)]. The front of the air pocket continues to move toward the vertical riser [Fig. 2(d)].

Figs. 3(a and b) show the typical pressure variation at two different points of the tunnel for an experiment (Series A, Run A1) with $D_r = 16$ mm: Point A—at the soffit of the downstream end of the pipe; Point B—at the invert level just beneath the vertical riser (cf. Fig. 1). Without an independent external head, the pressure in the tunnel is provided by the water column in the riser only. Fluctuation in the pressure can be observed after opening the valve. The maximum pressure created is approximately the same as the initial water depth in the riser [Fig. 3(a)]. The water level in the riser drops at first because of the compression of the air pocket, and fluctuates at approximately $0.65H_0$ [Fig. 3(b)]. The CFD prediction allows the estimation of the volume of air in the system, by summing up the product of the volume of computational cell and the air volume fraction inside. The variation of air volume is approximately 5–10% of the total volume of entrapped air [Fig. 3(c)]. The pressure fluctuation and water-level variation at the riser are gradually damped owing to the friction of the pipe and riser, until the air pocket reaches the riser at $T_a = 7.7$ s, after which the pressure decreases monotonically. The pressure variation at Point A is very similar to that at the base of the riser.

A very different pressure variation results if an upstream constant pressure head is imposed (Run B1, Fig. 4). At point A [Fig. 4(a)], the pressure increases sharply after the start of simulation because of the compression of the air pocket by the upstream pressure. The reduction in air volume is approximately 10% at maximum [Fig. 4(d)], but it already creates the increase in gauge pressure of approximately 1.7 times the upstream head. The pressure variation at point B [Fig. 4(b)] is smaller, approximately 1.5 times the upstream head. The water level at the riser also fluctuates because of the pressure variation [Fig. 4(c)]. The computed pressure variation in general compares well with the measurements at the same locations in the physical experiment, although the predicted damping of the pressure fluctuation is somewhat greater than observed—possibly attributable to the uncertainty in the pipe roughness. The significant pressure variation after the arrival of the air pocket ($T_a = 7.8$ s) can be clearly noted.

Simulated Flow Field in Riser for Geyser Event

Rise of Air Pocket in the Riser

Fig. 5(a) shows the computed air-water interaction after the air pocket arrives at the vertical riser for $D_r = 16$ mm without an upstream head (Run A1; Series A). The air pocket arrives at the riser at $T_a = 7.7$ s. Only part of the air enters the riser; whereas the remaining air keeps advancing upstream. The air pocket in the riser resembles a steadily rising Taylor bubble; a small (~0.2 m) rise in the free-surface level can also be noted. Owing to the film flow around the air pocket, the water column above the pocket decreases steadily. At $t = 9.7$ s, the air pocket breaks the free surface. The

J. Hydraul. Eng., 2018, 144(3): 04017071

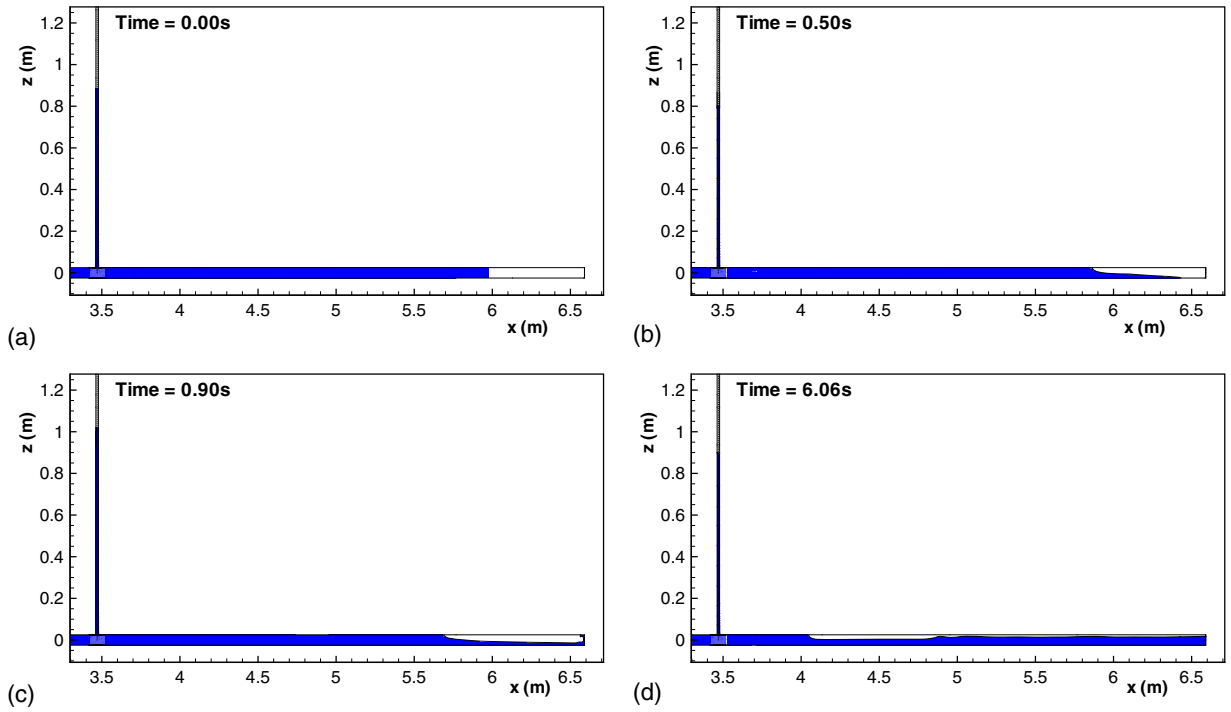

Fig. 2. Air pocket propagation in the tunnel with riser diameter of 16 mm, Series B (Run B1, with upstream head $H_0 = 0.88$ m, $L_0 = 0.61$ m): (a) $t = 0.0$ s; (b) $t = 0.5$ s; (c) $t = 0.9$ s; (d) $t = 6.0$ s

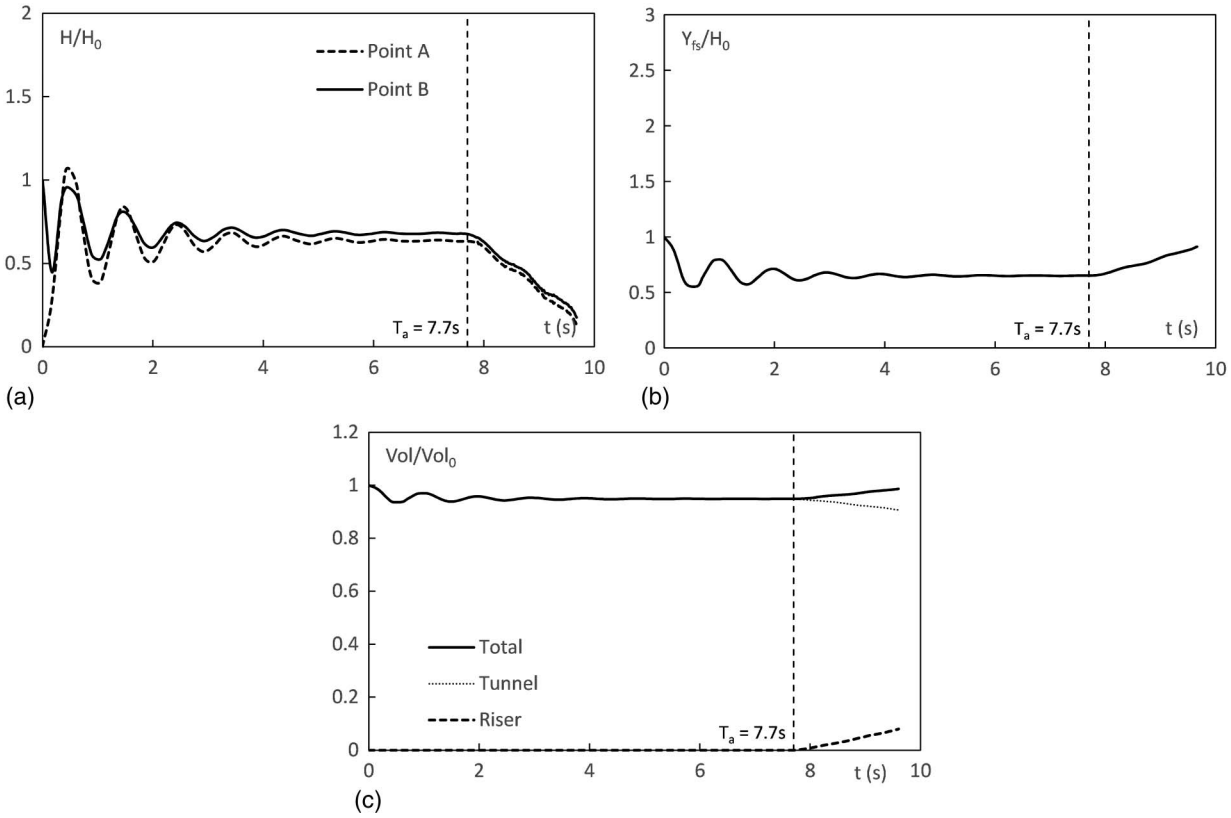

Fig. 3. (a) Pressure at Points A and B; (b) free-surface level at riser; (c) air volume of Run A1, $D_r = 16$ mm without an upstream pressure head (Series A); T_a is the time when the air pocket arrives at the riser; $H_0 = 0.88$ m is the initial water depth in the riser

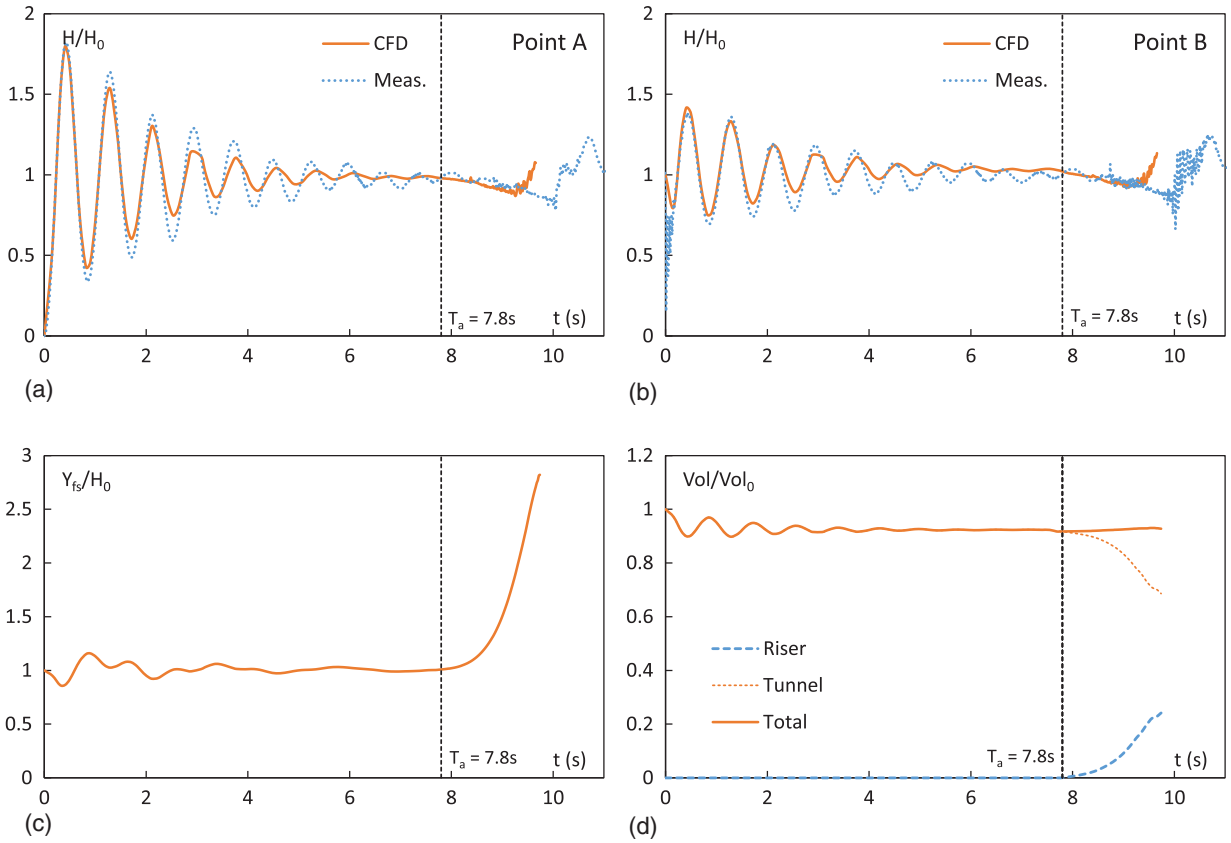

Fig. 4. (a) Pressure at Point A; (b) pressure at Point B; (c) free surface level at riser; (d) air volume of Run B1, $D_r = 16$ mm (Series B); T_a is the time when the air pocket arrives at the riser; $H_0 = 0.88$ m is the upstream pressure head

pressure in the tunnel drops steadily as the air pocket rises [Fig. 3(a)]. The volume of air in the system increases back to the initial volume as the pressure compression action ceases [Fig. 3(c)].

On the other hand, Fig. 5(b) shows the simulated fluid motion after the air pocket arrives at the vertical riser for $D_r = 16$ mm with an upstream head (Run B1, Series B). Whereas the initial horizontal air pocket propagation is similar to that for the Series A experiment, after some time, the nose of the air pocket undergoes a fast vertical acceleration, resulting in a rising speed much greater than that of a Taylor bubble. The free surface is pushed by the air pocket to rise rapidly, until the bubble breaks the free surface. The main air pocket is followed by a trailing mixture of air and water that enters the riser from the tunnel—much like a churning flow (Wallis 1969). In the corresponding physical experiment a geyser is observed, and the water is ejected out of the experimental riser (height = 1.8 m; Cong et al. 2017). The pressure in the tunnel drops steadily as the air pocket rises, but rises again when water enters the riser at approximately $t = 9$ s [Figs. 4(a and b)]. The volume of air in the system remains more or less unchanged [Fig. 4(d)] compared with that when the air enters the riser.

Fig. 6(a) shows the level of the free surface level in the riser Y_{fs} and the nose of the air pocket Y_{int} for the case without upstream head (Run A1, Series A). The rising speed of the interface and free surface are quite steady. The net rising speed of the front of the air pocket (relative to the free surface) is somewhat larger than that for the Taylor bubble (Davies and Taylor 1950), i.e., $V_{\text{Taylor}} = 0.345\sqrt{gD_r}$; however, the pressure inside the air pocket closely resembles that of the hydrostatic pressure induced by the water column of length L_w above [Fig. 6(b)].

Fig. 7(a) shows the level of the free surface at the riser Y_{fs} and the nose of the air pocket Y_{int} for the case of a geyser (Run B1, Series B). After entry into the riser, the initial rising speed of air pocket follows the Taylor bubble speed. At approximately 9 s, there is a significant acceleration in the rising speed of Y_{int} and Y_{fs}. The predicted trajectory of the free surface and interface is in general consistent with the measurement from high speed imaging. The average air pressure in the air pocket in the riser from the CFD simulation is much greater than the hydrostatic pressure of the overlying water column during the event of geyser [Fig. 7(b)]. It is shown from vertical momentum conservation of the water column in the riser (Cong et al. 2017) that this pressure difference creates an acceleration to push out the water column from the riser. It is also observed that a larger volume of air enters the riser for the geyser event (Run B1) as compared with the case without a geyser (Run A1).

Water Film around the Air Pocket

Fig. 8 illustrate the simulated flow field of the air pocket and the surrounding film flow. When the air pocket rises like a Taylor bubble (Run A1, Series A), the head of the bubble is more round-shaped [Fig. 8(a)]. The average film flow velocity can be estimated using the flow rate of water divided by the area occupied by the water film in a cross section. By the unit film flow theory (Batchelor 1967), the average steady falling velocity of the film v_f (relative to the free surface) and the film flow thickness δ can be estimated, respectively, as:

$$v_f = \frac{g\delta^2}{3\nu} = 0.27a\left(\frac{g^2}{\nu}\right)^{1/3} \tag{6}$$

$$\delta = 0.9a\left(\frac{\nu^2}{a^3 g}\right)^{1/6} \tag{7}$$

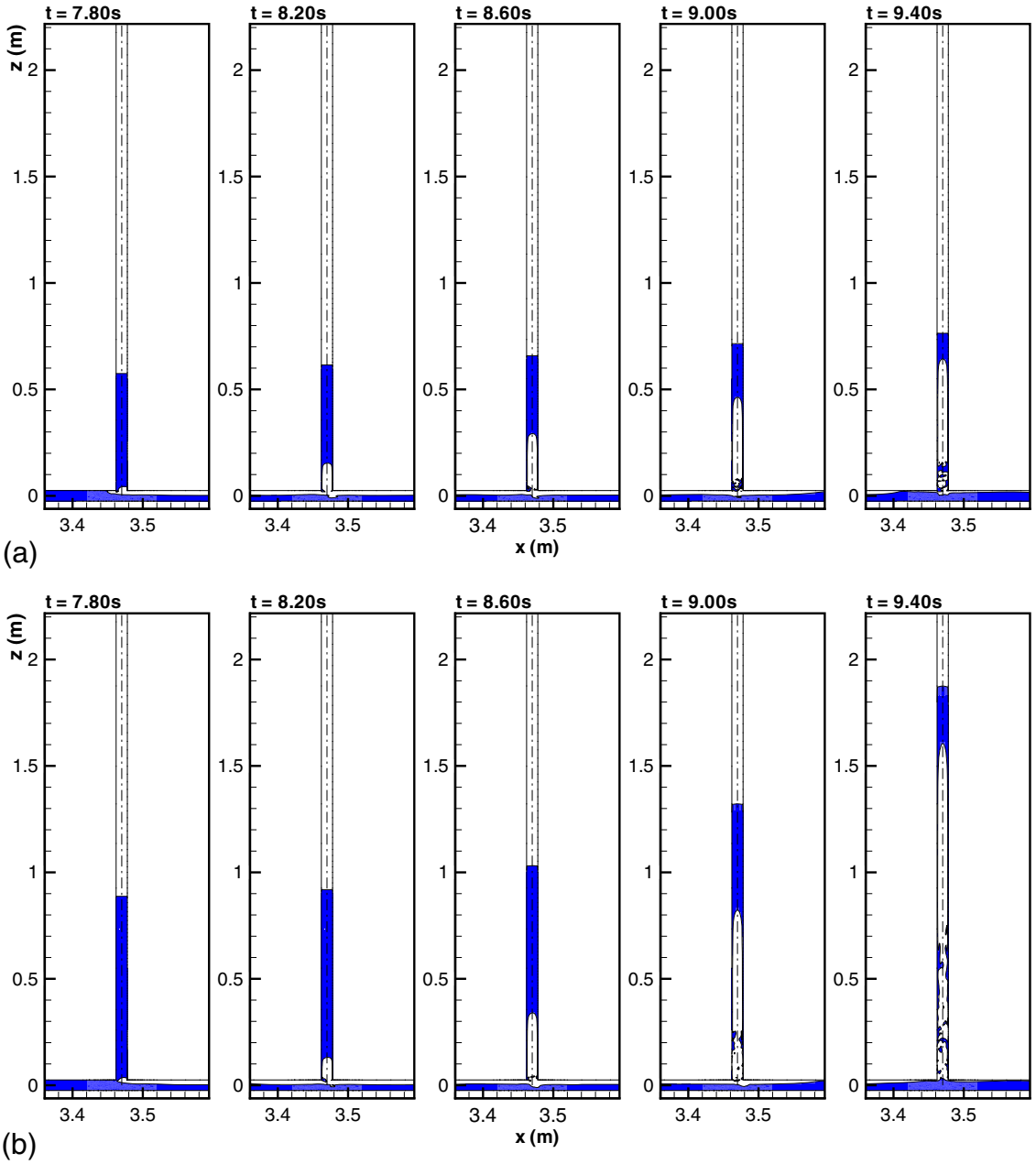

Fig. 5. Predicted rise of air pocket in the riser for $D_r = 16$ mm: (a) Run A1–without pressure head; (b) Run B1–with pressure head

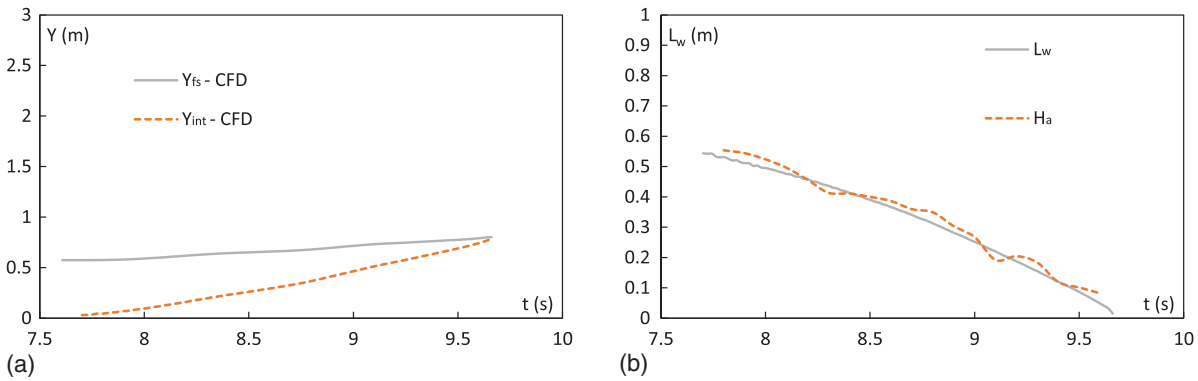

Fig. 6. (a) Level of free surface Y_{fs} and interface Y_{int}; (b) length of water column above air pocket L_w and air pressure ($H_a = P_a/\rho_w g$) for $D_r = 16$ mm, Run A1, without external pressure head

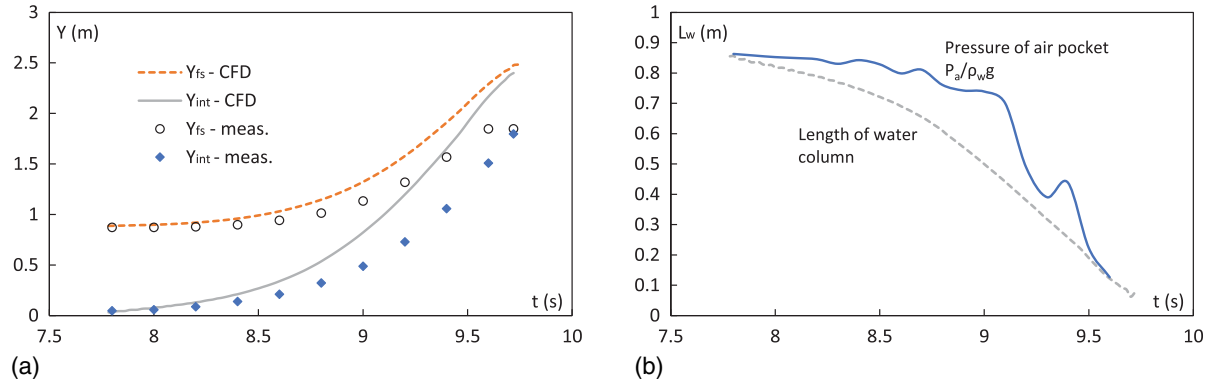

Fig. 7. (a) Level of free surface Y_{fs} and interface Y_{int}; (b) length of water column above air pocket L_w and air pressure ($H_a = P_a/\rho_w g$) for $D_r = 16$ mm, Run B1, with a pressure head $H_0 = 0.88$ m

where a = radius of the riser, and $\nu = 10^{-6}$ m^2/s = kinematic viscosity of water. For a riser diameter of $D_r = 16$ mm, the theoretical film flow velocity v_f is estimated to be 0.99 m/s and the film thickness is 0.55 mm. Film flow thickness predicted by CFD is approximately 0.8 mm, which is consistent with the theoretical predictions and the measurement in Cong (2016), despite of the uncertainties in predicting the interface between water and air. It is also noted that during a geyser event (Run B1, Series B) the air pocket head is more elongated and bullet-shaped (Fig. 8). The air flow is much stronger for the case of a geyser event, with velocities an order of magnitude greater than the corresponding flow field without geyser (Run A1).

Simulated Flow Field in Riser: Cases without Geyser Occurrence

Fig. 9 shows the simulation for a case with a larger riser diameter, $D_r = 40$ mm (Run B14, $D_r/D = 0.8$). In this case, the simulations does not reveal a geyser event—with or without the prescription of an upstream head. As the air pocket reaches the vertical riser, almost the entire air pocket enters the riser with no or negligible horizontal upstream air propagation past the riser. In Series A (Run A2), the air pocket rises like a Taylor bubble, with a small vertical rise of the free surface. In Series B (Run B14), both the air pocket and the free surface rise more rapidly, but the air-pocket motion relative to the free surface is still similar to that of a Taylor bubble. At $t =$ 5.3 s, more air enters the riser, and the trailing edge of the air pocket is an air-water mixture that resembles a churning flow (Wallis 1969). This influx of air-water mixture results in the rapid acceleration of the air pocket. On the other hand, in the corresponding Series A experiment (without independent upstream head), the falling water film just flows around the air pocket down the riser. The pressure in the air pocket in the riser is approximately the same as the hydrostatic pressure of the overlying water column, although some fluctuations can be noted (Fig. 10).

For the cases without an independent upstream pressure head (Run A2), as the water in the vertical riser is displaced by the rising air pocket, the pressure continuously decreases during the ascent of the air pocket. There is no external pressure that could result in the compression of air in the riser; thus, a rapid acceleration of the air pocket (geyser) would not occur.

Overall, based on the simulations of the 18 cases (with and without independent pressure head, Table 1), the following points can be made: (1) the broad features of the observed air pocket migration within the riser and the geyser dynamics are well simulated by the 3D CFD model. The occurrence of a geyser event is indicated by rapid acceleration of the water column, under conditions that reflect a compressed air pocket with pressure far exceeding the hydrostatic pressure of the water column above; (2) consistent with the experiments, geysers are not simulated in the Series A runs; and (3) details of the pressure variation and air pocket speed differ somewhat from the observations; this may be attributed to the assumed initial condition (instantaneous valve opening) and the inability of the turbulence model to accurately model the complex two-phase flow phenomenon.

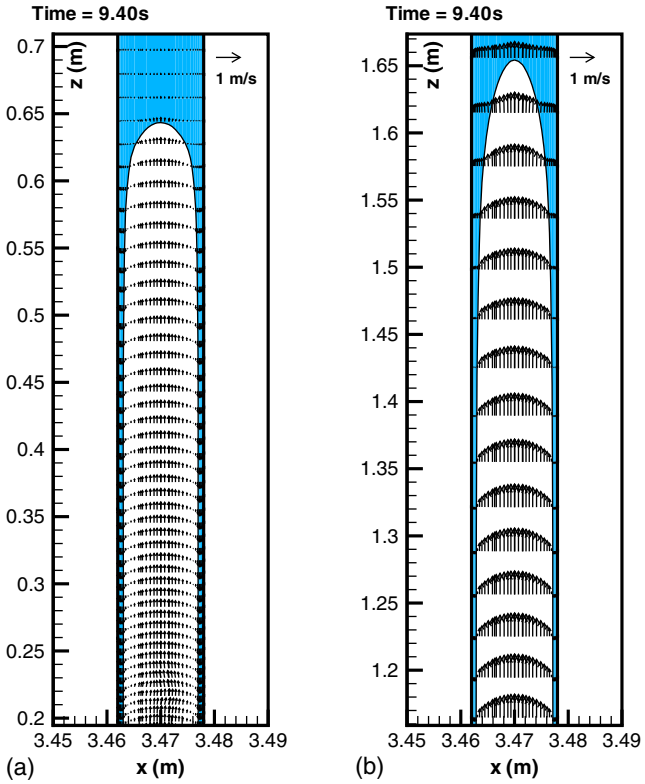

Fig. 8. Computed velocity field around the rising air pocket in the riser for: (a) Run A1, Series A–no upstream head (no geyser); (b) Run B1, Series B–with upstream head (geyser occurred). $D_r = 16$ mm, $H_0 = 0.88$ m

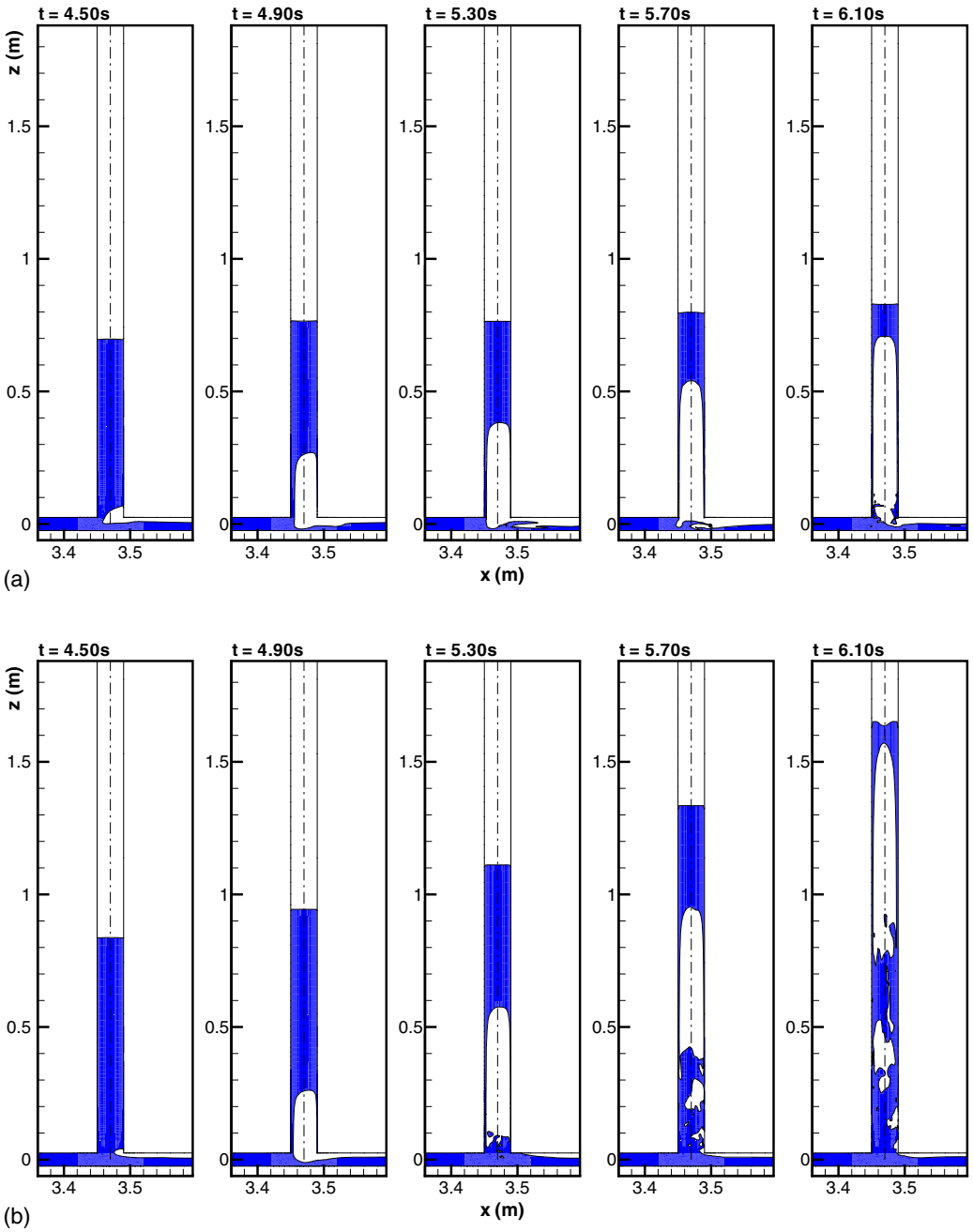

Fig. 9. Predicted air pocket migration in vertical riser, $D_r = 40$ mm (no geyser): (a) Run A2–without pressure head; (b) Run B14–with pressure head

Comparison of Numerical Predictions with Experiments of Lewis

The CFD model is also applied to simulate a geyser event observed in the experiments of Lewis (2011), for which data are available. The experimental set up is similar to that of Cong et al. (2017), but approximately twice larger. A large constant-head reservoir is connected to the upstream end of the tunnel; the diameter of the tunnel is $D = 0.095$ m; the riser diameter is $D_r = 0.044$ or 0.095 m ($D_r/D = 0.46$,1.00). The riser is located at 1.70 m downstream of the reservoir. A valve located at 3.78 m downstream of the riser separates a closed section of air of length $L_0 = 0.89$ m from the water in the horizontal pipe and riser. The air volume is adjusted by partly filling up the closed section with water. Various combinations of reservoir level $H_0 = 0.203$,0.457 m above the invert and the air pocket volume of 1.59, 3.14, and 5.97 L are tested. The air-water interface and the free surface are analyzed from recorded video images.

The CFD model is applied for the case of $D_r = 0.44$ m ($D_r/D = 0.46$), $H_0 = 0.457$ m, air volume = 5.97 L, for which a geyser is observed (Run B16). Fig. 11(a) shows the computed air-water interface in the horizontal tunnel and vertical riser at $t = 9$ s. The trapped air pocket near the tunnel-riser junction is seen; it is found that the air pocket does not entirely enter the vertical riser; part of the air pocket intrudes upstream past the riser junction [Fig. 11(a)]. The predicted free surface and air-water interface levels in the riser are in good agreement with the data of Lewis (2011) [Fig. 11(b)]. It is also found that the air pressure during this geyser event is significantly higher than that of the water column above, resulting in the acceleration of the water column [Fig. 11(c)].

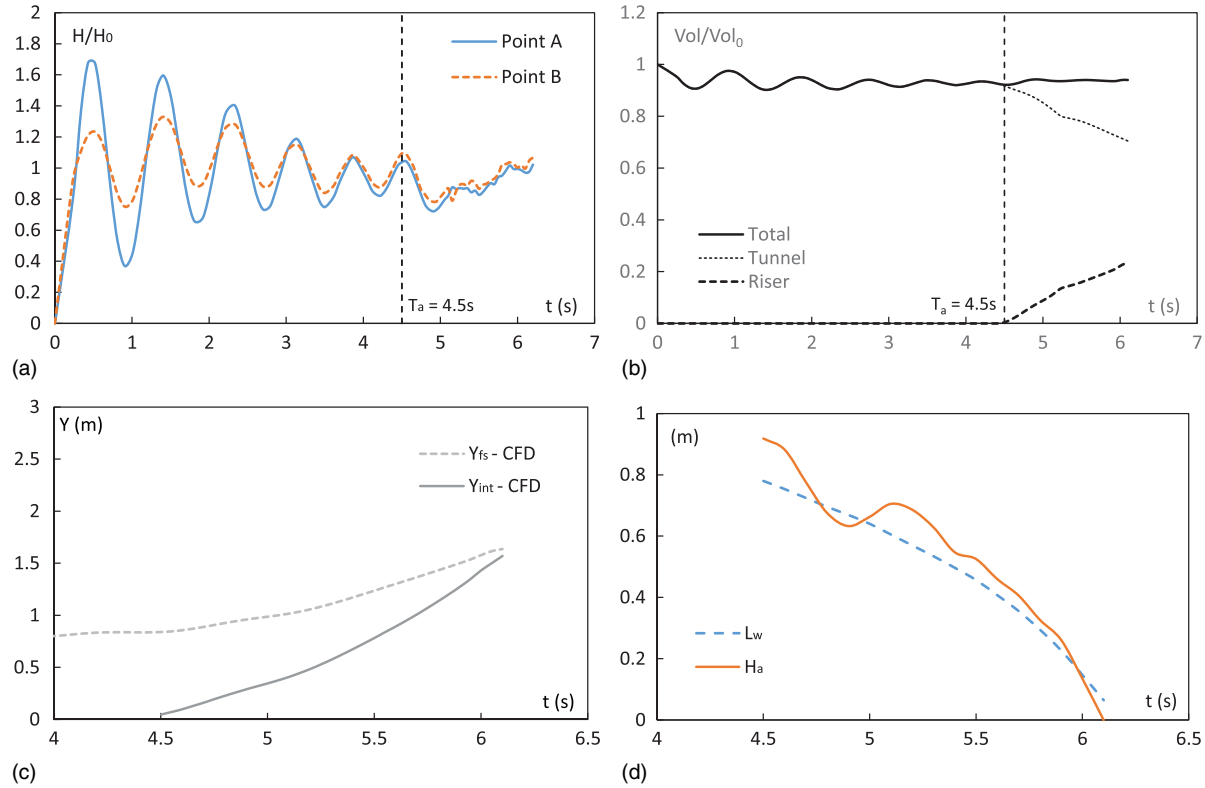

Fig. 10. (a) Predicted pressure at Points A and B; (b) air volume; (c) free-surface level Y_{fs} and air-pocket tip level Y_{int} in riser; (d) water-column length L_w and air-pocket pressure H_a for Run B14, $D_r = 40$ mm and $H_0 = 0.88$ m, with an upstream pressure head (Series B); T_a is the time when the air pocket arrives at the riser

Effect of Shaft Diameter on Geyser Formation

Using the validated CFD model, the effect of shaft diameter, air pocket volume and upstream pressure head on the formation of the geyser can be studied. A relatively coarse mesh (approximately 40,000 grid cells in total) is used for systematic numerical testing. In general, the numerical predictions are consistent with the experimental observations.

The results for the maximum height of the riser of the water column in the riser, defined as the level where the air pocket breaks through the free surface, are presented in Table 1. It is found that in general the height of the rise of the water column increases for the smaller riser diameter, larger upstream head and larger entrapped air volume. For the same upstream pressure head of 0.66 m and air volume of $L_0 = 0.61$ m, the height of the rise decreases from 1.5 m at $D_r = 0.021$ m (Run B2) to 1.09 m for $D_r = 0.04$ m (Run B12). Analysis of the pressure in the air pocket in the vertical riser suggests that for $D_r = 0.016, 0.021, 0.026$, and 0.031 m (Run B1–B10), the air pressure can be significantly larger than the overlying hydrostatic pressure under some conditions. On the other hand, for $D_r = 0.036$ and 0.04 m (Run B11–B15), the air pressure head is always approximately given by the length of the overlying water column (see Fig. 12 for four of the cases with the same pressure and air pocket volume). The extensive numerical simulations reveal the rapid acceleration of the water column (and hence a possible geyser event) for $D_r \le 0.031$ m (or $D_r/D \le 0.62$); this criterion is generally consistent with a heuristic analysis of the experimental observations (Cong et al. 2017). It is noteworthy that for $D_r = 0.021$ m and 0.026 m [Run B2 and B3, Figs. 12(a and b)], the air pressure is always larger than the hydrostatic pressure, whereas for $D_r = 0.031$ m [Run B5, Fig. 12(c)] there exists significant pressure fluctuation; at times the air pressure is the same as the hydrostatic pressure, whereas at other times it differs. The pressure fluctuation is a reflection of the complexity of the air-water interaction; it may be interpreted as transient owing to the compression/dilation of the air pocket and gradual damping of the oscillation during the ascent of the air pocket.

Effect of Upstream Pressure and Air Pocket Volume on Geyser Formation

The effect of upstream pressure and air-pocket volume on geyser formation are also studied for Series B cases. With the same riser diameter, the maximum height of rise of the water column increases with increasing pressure head H_0 and initial air volume $(\pi D^2/4)L_0$. A larger upstream pressure indicates that the air pocket is more compressed in the tunnel. H_0 also represents the length of the water column inside the riser and the length that the air pocket has to penetrate through. The maximum height of rise increases from 0.96 to 1.64 m for $H_0 = 0.5$–1.0 m with $D_r = 0.031$ m and $L_0 = 0.61$ m (Run B4–B7). The height of rise is always larger than that of the pressure head H_0. Fig. 13 shows the pressure variation for the cases of $H_0 = 0.50$, 0.88, and 1.0 m (Run B4, B6, and B7). It is interesting to note that the pressure is similar to the hydrostatic one, without the fluctuations as observed in the case of $H_0 = 0.66$ [Run B5, Fig. 12(b)]. Such observation reflects that a higher pressure results in a longer water column (larger mass above the air pocket) in the riser resulting in smaller accelerations (for the same air pressure). For cases which geysers occur (Run B5–B7), the net air pocket rising speed is generally larger than the cases without geyser (Run B4, Table 1).

On the other hand, an increase in air volume always lead to a higher potential for geyser formation. From Table 1, the maximum height of rise of the air pocket increases with the initial air volume

J. Hydraul. Eng., 2018, 144(3): 04017071

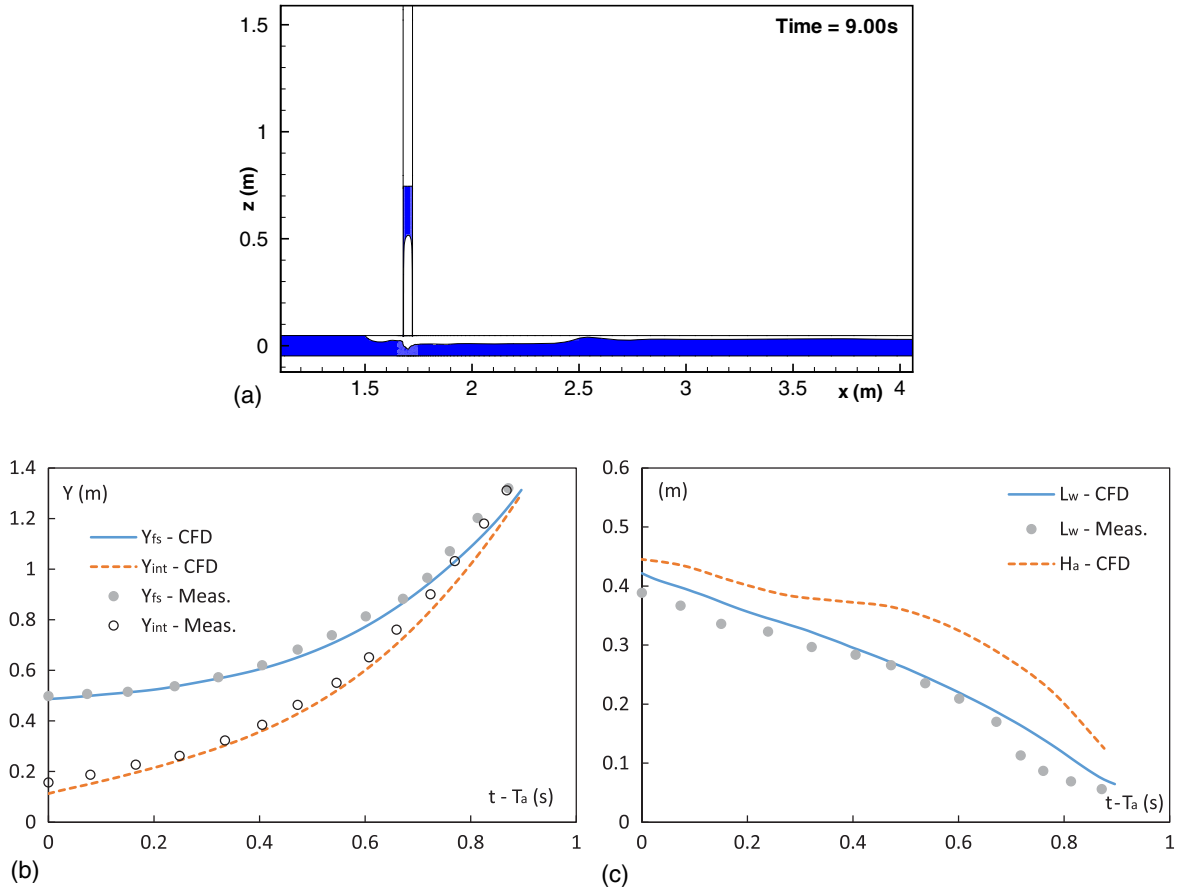

Fig. 11. (a) Predicted dynamics of air pocket for $D_r = 44$ mm, $D = 95$ mm with an upstream pressure head $H_0 = 0.46$ m (Run B16, experimental data of Lewis 2011); (b) predicted and observed free-surface level Y_{fs} and interface level Y_{int}; (c) predicted and observed water-column length L_w and air-pocket pressure H_a

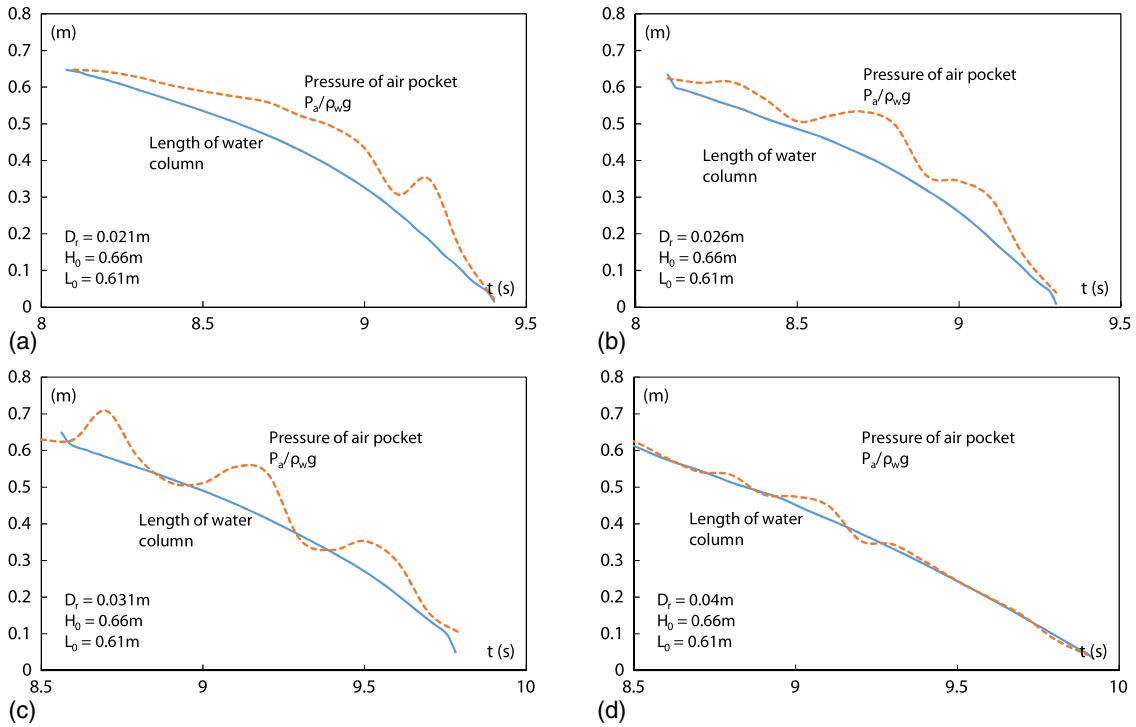

Fig. 12. Effect of riser diameter D_r on pressure variation in the air pocket for $H_0 = 0.66$ mm, $L_0 = 0.61$ m: (a) $D_r = 0.021$ m (Run B2); (b) $D_r = 0.026$ m (Run B3); (c) $D_r = 0.031$ m (Run B5); (d) $D_r = 0.04$ m (Run B12)

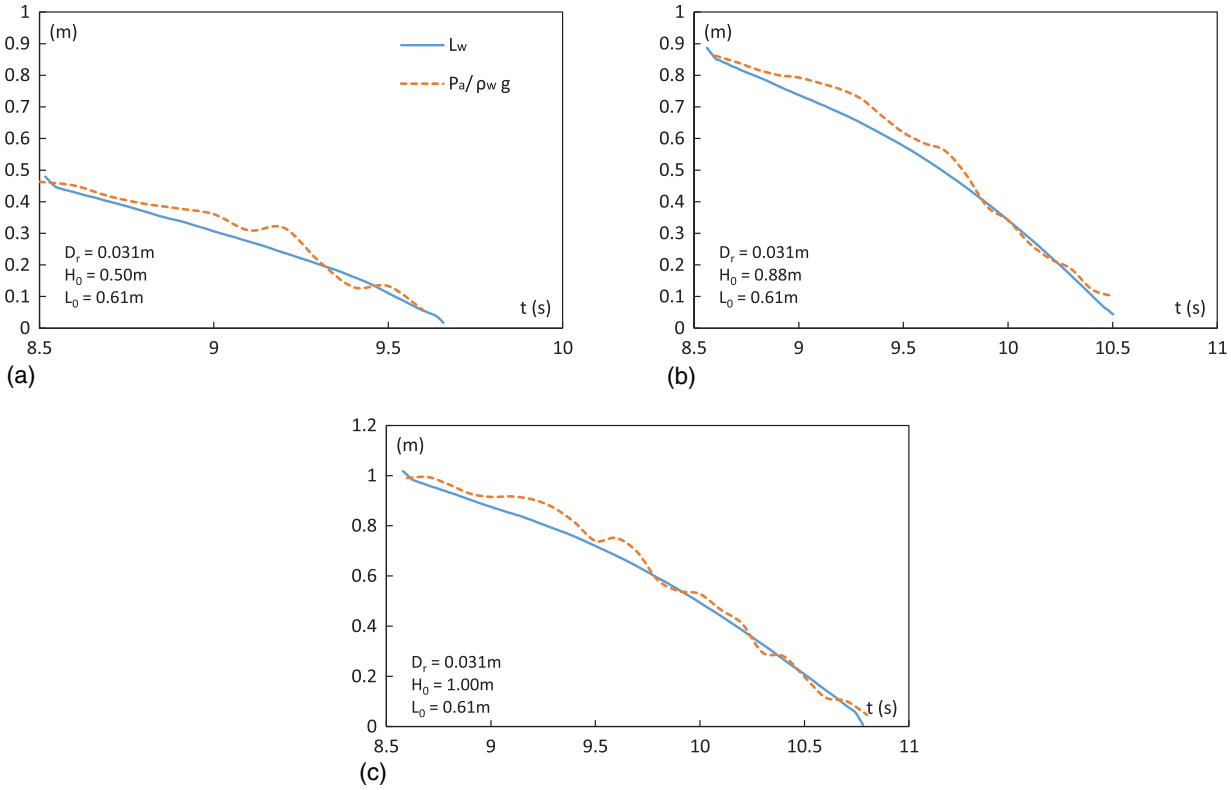

Fig. 13. Effect of upstream head H_0 on pressure variation in the air pocket for $D_r = 31$ mm, $L_0 = 0.61$ m: (a) $H_0 = 0.50$ m (Run B4); (b) $H_0 = 0.88$ m (Run B6); (c) $H_0 = 1.00$ m (Run B7)

for both $D_r = 0.031$ m and 0.04 m. For example, for the case of $D_r = 0.031$ m and $H_0 = 0.88$ m, the maximum height of rise increases from 1.52 to 1.82 m with a tripling of the air pocket volume (Run B6 versus B9). For the case of $D_r = 0.04$ m, the height of rise increases from 1.09 to 1.21 m with a tripling of the air pocket volume for $H_0 = 0.66$ m (Run B12 versus B13), and increases from 1.57 to 1.68 m with an increase in the air pocket volume by 22% for $H_0 = 0.88$ m (Run B14 versus B15). Significant pressure difference between the air pressure and the hydrostatic pressure for the cases of larger volume is also observed (not shown).

3D Numerical Modeling of Prototype Geyser

The numerical model is particularly useful in studying air-water interactions and the possible occurrence of geysers in a highly idealized drainage system that is broadly similar to the laboratory experiment but extrapolated to prototype dimensions. An attempt to study prototype geyser behavior is made by using the dimensions of the system similar to that at a location where a geyser event has been observed in Minneapolis, Minnesota; field measurements collected during a rainfall event on July 11, 2004, have been reported in Wright et al. (2011). The diameter of the tunnel and the riser manhole are $D = 3.66$ m and $D_r = 2.44$ m ($D_r/D = 0.67$), respectively. The tunnel invert is located at 28.6 m below grade at the location of the manhole. From the pressure record, the maximum water level at the manhole is approximately 6 m above the invert of the tunnel. The flow rate during the geyser event is estimated to be approximately 9 m^3/s, thus the estimated average flow velocity in the tunnel is $U_a = 0.86$ m/s. The time interval during each geyser event is approximately $T = 1$–1.5 min; assuming the existence of

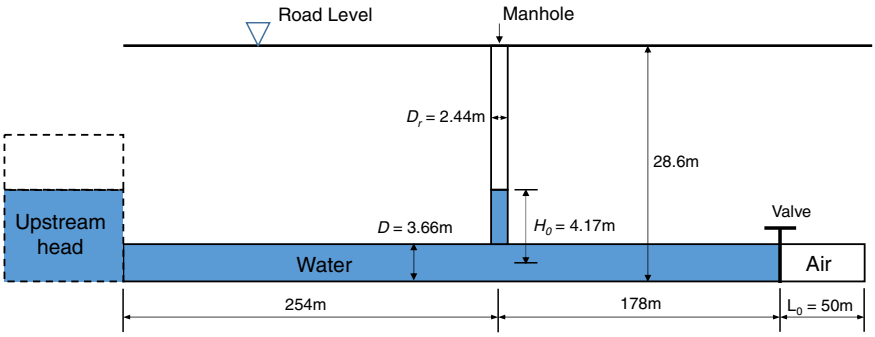

Fig. 14. Initial condition of a numerical experiment of geyser formation in a hypothetical prototype tunnel-dropshaft system; a pressure of $P_{a,t=0} = P_{\text{atm}} + \rho_w g H_0$ is prescribed in the air pocket; simulation starts by opening the valve and the air pocket propagates toward the dropshaft, leading to a geyser event

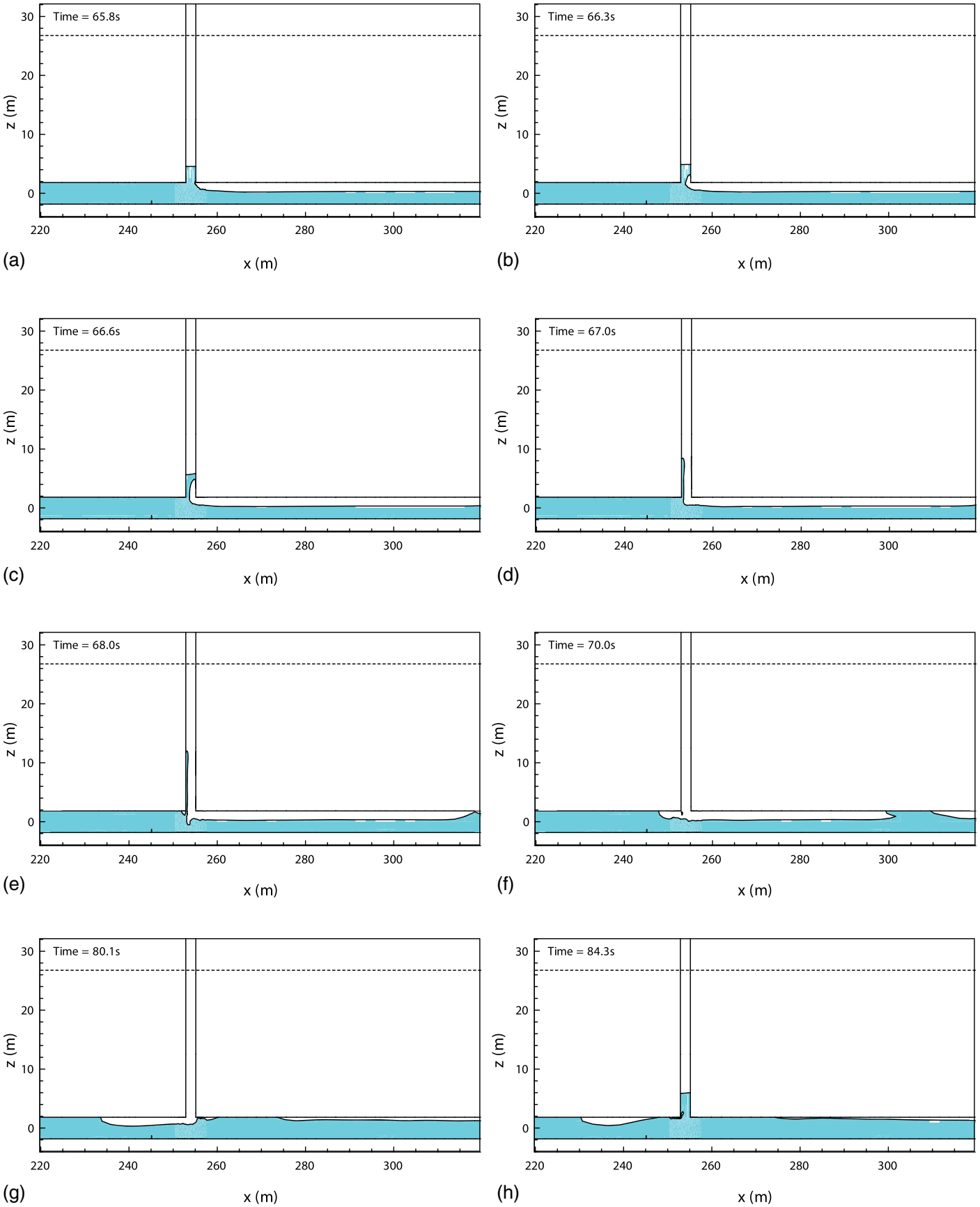

Fig. 15. CFD predicted air-water interaction in a numerical experiment of a hypothetical prototype tunnel-dropshaft system; the dash line indicates the ground level: (a) $t = 65.8$ s; (b) $t = 66.3$ s; (c) $t = 66.6$ s; (d) $t = 67.0$ s; (e) $t = 68.0$ s; (f) $t = 70.0$ s; (g) $t = 80.1$ s; (h) $t = 84.3$ s; geyser event occurs at $t = 67.0$ s

an air pocket that occupies the upper half of the tunnel; the length of an air pocket can be estimated from the flow velocity and the time interval between geyser events, $L_0 \approx U_a T \approx 50$–$100$ m (i.e., an air pocket volume in the order of 400 m^3). Recent numerical model investigations by Vasconcelos and Wright (2016) have demonstrated that depending on the storm water inflow patterns and system configuration, trapped air pocket volumes in the order of 1,000 m^3 can be found in prototype drainage systems.

In the CFD simulation of a prototype analog of the laboratory experiment, the volume of air at the end of the pipe is specified (Fig. 14). This corresponds to a prototype/model length scale of 73.2 when compared with the laboratory model of Cong et al. (2017), with $D_r = 0.05$ m. The initial air pocket length L_0 is 50 m.

The upstream pressure head is taken as 6 m above the tunnel invert level, i.e., 4.17 m above the tunnel centerline level. It is noted that under such pressure, the air volume is reduced by 30–40% according to the ideal gas law, i.e., $PV =$ constant. This is very different from the pressure head used in the laboratory study (less than 1 m), with reduction in the air volume of approximately 10%. In the simulation, the initial static pressure in the air pocket is prescribed as the hydrostatic pressure induced by the upstream head ($P_{a,t=0} = P_{\text{atm}} + \rho_w g H_0$) to balance the upstream head pressure and minimize the pressure oscillation induced by valve opening.

Fig. 15 shows the predicted air-water interaction in the tunnel and riser. Fig. 16 shows the predicted time variation of free surface and air-water interface in the riser [Figs. 16(a and b)], the predicted pressure at the invert of the tunnel below the dropshaft [Fig. 16(c)], and the velocity at 30 m above the tunnel centerline. The air pocket arrives at the dropshaft at $t = 65.8$ s [Fig. 15(a)]. The rising of the air pocket takes approximately 1 s [Figs. 15(b and c)] and breaks the water surface at $t = 67$ s [Fig. 15(d)]. At this instant, a large velocity of 20–30 m/s is induced in the dropshaft, causing the water film around the air pocket to be carried upward [Fig. 15(e)]. The water film falls back to the tunnel when the air velocity decreases after $t = 69$ s. The air pocket under high pressure is released through the dropshaft. The rear air-water interface in the tunnel moves upstream, resulting in the expulsion of the air volume from the dropshaft, whereas the upstream air-water interface is decelerated because of the upstream pressure [Figs. 15(f and g)]. Finally, the water fills up the dropshaft again [Fig. 15(h)].

The simulated mechanism of geyser formation in the prototype stormwater drainage system is similar to that in the laboratory experiment in several ways: The horizontal propagation of the air pocket in the tunnel, and the air pocket entry into the riser with subsequent acceleration. The air pocket rises quickly to break the free surface, with the pressure of air the pocket much greater than the hydrostatic head of the overlying water column [Figs. 16(a and b)]. However, the strength of the geyser is much larger in the prototype owing to the compression of the air pocket by a pressure head of approximately 5 m. An instantaneous velocity in the

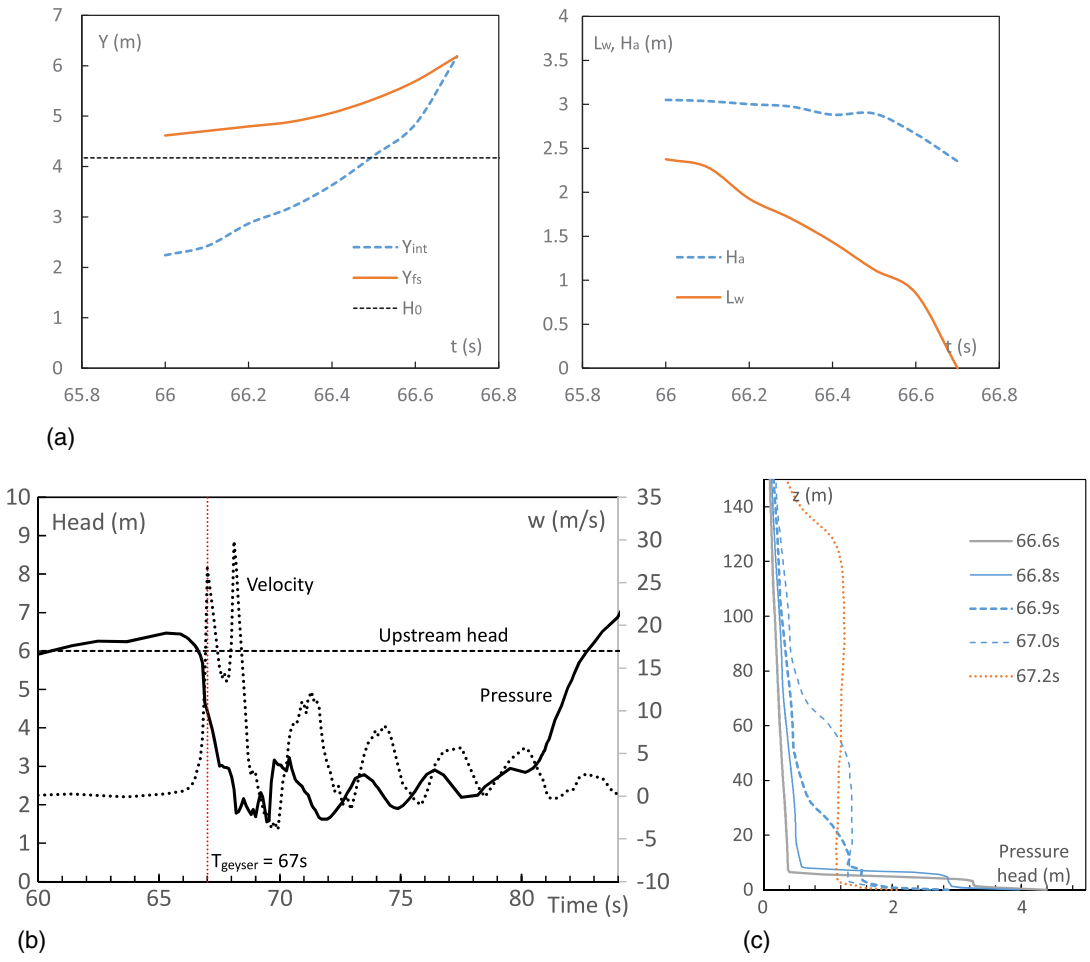

Fig. 16. CFD predicted characteristics of a geyser event in hypothetical prototype system: (a) level of interfaces (relative to tunnel centerline) and pressure in the air pocket; (b) pressure (solid line) and velocity (dashed line) variation, respectively, at the invert below the tunnel-riser junction and 30 m above the tunnel in the dropshaft; (c) pressure-head variation with height in the drop shaft

J. Hydraul. Eng., 2018, 144(3): 04017071

order of 20–30 m/s is generated attributable to the pressure gradient between the compressed air pocket and the atmosphere when it breaks through the water surface [Fig. 16(b)]. The pressure variation [Fig. 16(c)] at the dropshaft centerline shows that during the geyser, a pressure transient is formed and propagates up the dropshaft, in less than 1 s. According to a classification of two-phase flow regimes in a vertical tube (Taitel et al. 1980), such large typhoon/hurricane scale vertical velocity (in excess of ~10 m/s) can result in the breaking up of water into small droplets and the formation of a dispersed air-water mixture that is brought to the road surface. The predicted velocity is consistent with the rough estimation by Wright et al. (2011) from the height of the rise of the geyser. The predicted pressure variation is also qualitatively similar to that measured by a sensor installed in the tunnel invert (Wright et al. 2011).

Conclusions

A comprehensive 3D numerical study on the physics of geyser events is conducted using a CFD model with the VOF technique. Extensive numerical simulations are conducted to study the air-pocket dynamics caused by release of trapped air from a horizontal tunnel into a vertical riser. The predicted pressure variation, the air-water interface, and the free surface level in the riser compare well with experimental measurements. A geyser event can be characterized by compression of the air pocket and rapid acceleration of the water column in the riser; a geyser event occurs for the smaller riser diameter ($D_r/D \leq 0.62$) for the case with a prescribed independent upstream constant pressure head. The rising speed of both the air pocket tip and the free surface at the riser is much greater than those for the cases without an independent upstream pressure head. The pressure inside the air pocket in the riser is much greater than the hydrostatic pressure attributable to the water column above, resulting in the water column being rapidly pushed out of the riser. For the case with a large riser diameter ($D_r/D > 0.62$), the net rising speed of the air pocket relative to the free surface is similar to that of a Taylor bubble, without a net acceleration created by a pressure difference. The extensive numerical simulations are in general agreement with the laboratory experiments; geysers are likely to occur for $D_r/D \leq 0.62$.

The effect of riser diameter, upstream pressure head, and initial air pocket volume on geyser formation is studied through numerical experiments. It is found that the strength of the geyser (as represented by the maximum height of rise of the water column) increases with smaller riser diameter, greater upstream head, and larger air pocket. The potential occurrence of a geyser, acceleration and ejection of the water column, can be reflected in the pressure in the air pocket in the vertical shaft—which will be significantly larger than the hydrostatic pressure. The CFD model has also offered important insights on the details of the geyser formation in a hypothetical prototype system. In particular, it is shown that compressed air pockets with pressure heads of approximately 5 m can lead to large vertical air velocities of the order of 20 m/s; such high velocities may be responsible for the explosive air-water mixtures ejected from manholes—geysers that are often observed in the field.

Acknowledgments

This research is supported by a grant from the Hong Kong Research Grants Council (Project 16205114) and in part by a project on Smart Urban Water Supply Systems (SUWSS) under the Theme-based Research Scheme.

Notation

The following symbols are used in this paper:

a = riser radius;
$Cr = u\Delta t/\Delta x$ = Courant number;
D = horizontal pipe diameter;
D_r = vertical riser diameter;
$\mathbf{g}$ = $(0,0,-9.81)$ m/s^2, gravitational acceleration;
H_0 = initial water levels in the riser (Series A) or upstream head (Series B), measured from invert of tunnel;
$H_a = P_a/\rho_w g$ pressure head in air pocket in riser;
L_0 = initial air length in the horizontal pipe;
$L_w = Y_{fs} - Y_{\text{int}}$ length of water column above the air pocket;
k = turbulent kinetic energy;
M_w = molecular weight of air;
P = gauge pressure;
P_a = average pressure in air pocket;
P_{atm} = atmospheric pressure;
P_{op} = operating pressure;
Pr = Prandtl number;
R = universal gas constant;
T = time interval of each geyser event in prototype;
T_a = time when air pocket arrives at the riser after valve opening;
t = time from the start of experiment;
$\mathbf{U} = (u, v, w)$ = velocity field;
U_a = average flow velocity in tunnel in prototype;
$V_a = \pi D^2 L_0/4$ initial air volume;
$V_w = \pi D_r^2 H_0/4$ initial volume of water in the riser;
v_f = falling velocity of water film;
v_{net} = net rising velocity of air pocket relative to the free surface;
v_{Taylor} = velocity of a Taylor bubble;
Y_{fs} = free surface level in the riser;
Y_{int} = frontal level of air pocket in the riser;
$\alpha_a = 1 - \alpha_w$ volume fraction of air;
α_w = volume fraction of water;
ϵ = turbulent kinetic energy dissipation rate;
Δt = computational time step;
Δx = computational grid size;
δ = water film thickness;
μ_t = turbulent dynamic viscosity of air–water mixture;
ρ = air–water mixture density;
ρ_a = air density;
ρ_w = water density; and
ν = kinematic viscosity of water.

References

ANSYS FLUENT version 15.0 [Computer software]. ANSYS, Canonsburg, PA.

Batchelor, G. K. (1967). *Introduction to fluid dynamics*, Cambridge University Press, Cambridge, U.K.

Catano-Lopera, Y. A., et al. (2014). "Modeling of a transient event in the tunnel and reservoir plan system in Chicago, Illinois." *J. Hydraul. Eng.*, 10.1061/(ASCE)HY.1943-7900.0000888, 05014005.

Cong, J. (2016). "Experimental modeling of air-water interaction in horizontal pipe with vertical riser." M.Phil. thesis, Hong Kong Univ. of Science and Technology, Hong Kong.

Cong, J., Chan, S. N., and Lee, J. H. W. (2017). "Geyser formation by release of entrapped air from horizontal pipe into vertical

shaft." *J. Hydraul. Eng.*, 10.1061/(ASCE)HY.1943-7900.0001332, 04017039.

Davies, R. M., and Taylor, G. I. (1950). "The mechanics of large bubbles rising through extended liquids and through liquids in tubes." *Proc. Royal Soc. London A*, 200(1062), 375–390.

Hamam, M. A., and McCorquodale, A. (1982). "Transient conditions in the transition from gravity to surcharged sewer flow." *Can. J. Civ. Eng.*, 9(2), 189–196.

Hirt, C. W., and Nichols, B. D. (1981). "Volume of fluid (VOF) method for the dynamics of free boundaries." *J. Comput. Phys.*, 39(1), 201–225.

Lewis, J. W. (2011). "A physical investigation of air/water interactions leading to geyser events in rapid filling pipelines." Ph.D. thesis, Univ. of Michigan, Ann Arbor, MI.

Li, J., and McCorquodale, A. (1999). "Modeling mixed flow in storm sewers." *J. Hydraul. Eng.*, 10.1061/(ASCE)0733-9429(1999)125:11(1170), 1170–1180.

Martin, C. S. (1976). "Entrapped air in pipelines." *Proc., 2nd Int. Conf. on Pressure Surges*, Vol. 2, City Univ., London, 15–27.

Taitel, Y., Barnea, D., and Dukler, A. E. (1980). "Modelling flow pattern transitions for steady upward gas–liquid flow in vertical tubes." *AIChE J.*, 26(3), 345–354.

Vasconcelos, J. G., and Wright, S. J. (2008). "Rapid flow startup in filled horizontal pipelines." *J. Hydraul. Eng.*, 10.1061/(ASCE)0733-9429(2008)134:7(984), 984–992.

Vasconcelos, J. G., and Wright, S. J. (2011). "Geysering generated by large air pockets released through water-filled ventilation shafts." *J. Hydraul. Eng.*, 10.1061/(ASCE)HY.1943-7900.0000332, 543–555.

Vasconcelos, J. G., and Wright, S. J. (2012). "Mechanisms for air pocket entrapment in stormwater storage tunnels." *Proc., World Water and Environmental Resources Congress 2006*, ASCE, Reston, VA.

Vasconcelos, J. G., and Wright, S. J. (2016). "Anticipating transient problems during the rapid filling of deep stormwater storage tunnel systems." *J. Hydraul. Eng.*, 10.1061/(ASCE)HY.1943-7900.0001250, 06016025.

Wallis, G. B. (1969). *One-dimensional two-phase flow*, McGraw Hill, New York.

Wright, S. J. (2013). "Influence of air pocket volume on manhole surge." *J. Water Manage. Model.*, 141–155.

Wright, S. J. (2014). "Modeling rapid filling processes in stormwater tunnel systems." *Proc., DSD 25th Anniversary Int. Conf.*, Hong Kong Drainage Services Dept., Hong Kong.

Wright, S. J., Lewis, J. W., and Vasconcelos, J. G. (2011). "Geysering in rapidly filling storm-water tunnels." *J. Hydraul. Eng.*, 10.1061/(ASCE)HY.1943-7900.0000245, 112–115.

Youngs, D. L. (1982). "Time-dependent multi-material flow with large fluid distortion." *Numerical methods for fluid dynamics*, Academic Press, Cambridge, MA.

Zhou, F., Hicks, F., and Steffler, P. M. (2002a). "Observations of air-water interaction in a rapidly filling horizontal pipe." *J. Hydraul. Eng.*, 10.1061/(ASCE)0733-9429(2002)128:6(635), 635–639.

Zhou, F., Hicks, F., and Steffler, P. M. (2002b). "Transient flow in a rapidly filling horizontal pipe containing trapped air." *J. Hydraul. Eng.*, 10.1061/(ASCE)0733-9429(2002)128:6(625), 625–634.

Zhou, L., Liu, D.-Y., and Ou, C.-Q. (2011). "Simulation of flow transients in a water filling pipe containing entrapped air pocket with VOF model." *Eng. Appl. Comput. Fluid Mech.*, 5(1), 127–140.